



CrossMark  
click for updates

HPSTAR  
093-2015

# Anomalous variation of electrical transport property and amorphization in dense Alq<sub>3</sub>

Cite this: *RSC Adv.*, 2015, 5, 41359

Feng Ke,<sup>ab</sup> Qinglin Wang,<sup>b</sup> Junkai Zhang,<sup>b</sup> Ying Guo,<sup>a</sup> Dayong Tan,<sup>bc</sup> Yan Li,<sup>a</sup> Cailong Liu,<sup>\*a</sup> Yonghao Han,<sup>a</sup> Yanzhang Ma,<sup>d</sup> Xiao-Jia Chen,<sup>b</sup> Bin Chen<sup>b</sup> and Chunxiao Gao<sup>\*a</sup>

Herein, we report the intriguing electrical transport and structural properties of compressed Alq<sub>3</sub>, which is an extensively used electron transport material in OLEDs. The bulk resistance ( $R_b$ ) of Alq<sub>3</sub> increases with uploading pressure, but drops markedly when the uploading pressure is above 8.6 GPa. In contrast, the grain boundary resistance ( $R_{gb}$ ) varies smoothly below 16.4 GPa. With further compression, both  $R_b$  and  $R_{gb}$  increase with the amorphization of Alq<sub>3</sub>. The pressure-induced amorphization is found to be reversible at a low density amorphous state, while it is irreversible at a higher density state. Interestingly, XRD measurements indicate no structural transition at  $\sim 8.0$  GPa. The variation of  $R_b$  is found to be synchronous with the blue-shift of the Al–oxine deformation mode, which rationalizes the anomalous changes of  $R_b$ . The Al–oxine interaction is believed to be also significant in the electrical transport properties of dense Alq<sub>3</sub>, which provides insight into the correlation between its structural changes and electrical transport properties.

Received 20th January 2015  
Accepted 23rd April 2015

DOI: 10.1039/c5ra01198a

www.rsc.org/advances

## Introduction

Since the first discovery of tris(8-hydroxyquinoline) aluminum (Alq<sub>3</sub>)-based multilayer thin-film electroluminescent devices by Tang and co-authors in 1987,<sup>1</sup> considerable progress has been made on their application in organic light-emitting devices (OLEDs) as electron-transporting materials.<sup>2–6</sup> In addition to the optimization of Alq<sub>3</sub>-based devices with higher efficiency and long-term stability, considerable theoretical and experimental effort has been focused on the polymorph and photo-physics properties of Alq<sub>3</sub>.<sup>7–15</sup> At room conditions, Alq<sub>3</sub> crystallizes into an octahedral coordinated chelate complex with Al<sup>3+</sup> at the center and three 8-hydroxyquinoline ions around it, which generally adopts two types of geometrical isomeric forms, namely, the meridional isomeric form (*mer*-Alq<sub>3</sub>) with  $C_1$  symmetry and facial isomeric form (*fac*-Alq<sub>3</sub>) with  $C_3$  symmetry, depending on the orientation of the ligands.<sup>15–22</sup> The structural difference between these two isomers is small, but considerably different physical properties, such as color and fluorescence, have been observed. The green emission for light-yellow *mer*-

Alq<sub>3</sub> and blue emission for whitish *fac*-Alq<sub>3</sub> have been attracting intensive interest of the scientists in the area of functional materials.

Recently, the spectral position of the fluorescence of Alq<sub>3</sub> was found to be correlated with both the molecular packing density and the length of interligand contacts between its neighboring molecules as a consequence of different dispersive and dipolar interactions as well as different  $\pi$ – $\pi$  orbital overlapping, *i.e.*, the denser the crystal is, the more red-shifted the fluorescence is.<sup>15</sup> This  $\pi$ – $\pi$  stacking interaction is also considered as a key factor for the electrical transport properties of Alq<sub>3</sub>, which is one of the most important physical properties in optimizing or designing new applications for organic functional materials.<sup>9,12–14</sup> For instance, in Alq<sub>3</sub>, large intermolecular electronic interactions, which depend on both intra- and intermolecular structures, are critical to its charge transfer rate and charge mobility.<sup>13</sup> An important issue concerns how to alter the optical and electrical transport properties of Alq<sub>3</sub> by tuning its intra- and intermolecular structure with external stimuli (*e.g.* pressure/temperature). As is well known, compression is a powerful tool to drive transformation towards the structures with higher density without inducing impurities or changing the chemical nature of materials,<sup>23</sup> which provides an approach to further explore the correlation between the structural and other physical properties of Alq<sub>3</sub>. Previous studies verified that the photoluminescence spectra of Alq<sub>3</sub> were indeed red-shifted considerably more than 0.3 eV.<sup>24–26</sup> Changes in electronic structure can fundamentally affect the electrical transport property of a material. Nevertheless, it remains unclear how

<sup>a</sup>State Key Lab for Superhard Materials, Institute of Atomic and Molecular Physics, Jilin University, Changchun 130012, China. E-mail: cailong\_liu@jlu.edu.cn; gaocx@jlu.edu.cn

<sup>b</sup>Center for High Pressure Science and Technology Advanced Research, Shanghai 201203, China

<sup>c</sup>Guangzhou Institute of Geochemistry, Chinese Academy of Sciences, Guangzhou 510640, China

<sup>d</sup>Department of Mechanical Engineering, Texas Tech University, Lubbock, TX 79409, USA

compression tunes the transport behavior of  $\text{Alq}_3$ , which limits the design of new  $\text{Alq}_3$ -based applications. Another factor that critically affects the performance of OLED lighting or display applications is the grain boundary or interface of crystalline materials. The carrier scattering effect is usually strengthened at grain boundaries, and thus changes the electrical transport properties of materials. The effect of the grain boundary on the electrical transport properties of  $\text{Alq}_3$  under compression is under investigated and thus poorly understood.

An effective approach to solve the above mentioned issues is the alternating current electrical response analysis, *i.e.*, frequency-dependent impedance spectroscopy, using which the contribution of the bulk and grain boundary effect on the total electrical transport properties can be distinguished. Furthermore, *in situ* high-pressure synchrotron X-ray diffraction (XRD) and Raman spectroscopy were conducted to monitor the structural modification, which is still not well-defined but of great importance for understanding the changes of physical properties of  $\text{Alq}_3$  under compression. Besides, high-resolution transmission electron microscopy (TEM) is applied to observe the pressure-induced change on the grain boundary of  $\text{Alq}_3$ . By combining these measurements, we have studied the electrical transport and structural properties of  $\text{Alq}_3$  under compression.

## Experimental section

Alternating current impedance spectroscopy measurements consist of a time ( $t$ )-dependent alternating voltage signal,  $U(\omega, t) = U_0 \cos(\omega t)$ , which is applied to a sample, and the current response signal,  $I$ , is determined as  $I(\omega, t) = I_0 \cos(\omega t - \gamma)$ , where  $\omega$ ,  $U_0$ ,  $I_0$  and  $\gamma$  are angular frequency, voltage amplitude, current amplitude and phase shift, respectively. Then, one can obtain complex impedance  $Z^* = U/I = Z' + iz''$ , in which the impedance fraction in phase with  $U(\omega, t)$  is defined as the real ( $Z'$ ) and the  $\pm\pi/2$  out of phase part is defined as the positive/negative imaginary part ( $Z''$ ), respectively. In our experiments, an a.c. voltage signal with the amplitude of 2 V and frequency ranging from 0.01 to  $10^7$  Hz was applied to the samples. A Solartron 1260 impedance analyzer, which was interfaced with a Solartron 1296 dielectric interface, was used to obtain the impedance spectra. Impedance spectra were measured with a two-electrode configuration microcircuit, in which an Mo film electrode was used as one of the probing electrodes and the sidewall of the sample chamber was used as the other. T301 steel was used as the gasket. The fabrication of the Mo film microcircuit on a diamond surface, the insulating method between the gasket and Mo film electrode, and other experimental details were reported previously.<sup>27,28</sup>

*In situ* high-pressure XRD measurements on  $\text{Alq}_3$  were conducted at beamline 4W2 of Beijing Synchrotron Radiation Facility (BSRF) and 15U1 of Shanghai Synchrotron Radiation Facility (SSRF) using an angle-dispersive XRD source ( $\lambda = 0.6199 \text{ \AA}$ ). Powdered  $\text{Alq}_3$  samples (bought from Sigma-Aldrich Co.) and a small piece of ruby as the pressure calibrant<sup>29</sup> were loaded into a diamond-anvil cell. Silicone oil was used as the pressure transmitting medium. The distance between the sample and detector, and detector parameters were calibrated

using a  $\text{CeO}_2$  standard. Bragg diffraction images were integrated using the Fit2d software, which yielded one-dimensional intensity *versus* diffraction angle  $2\theta$  patterns. High-pressure Raman spectra were obtained using a Renishaw InVia spectrometer using a 633 nm He-Ne laser and a  $50\times$  Leica optical microscope.

## Results and discussion

Fig. 1 shows the impedance spectral data of  $\text{Alq}_3$  powders with pressure of up to 19.4 GPa as the imaginary part of the complex impedance ( $Z''$ ) plot *vs.* that of the real part ( $Z'$ ). It is found that unlike the previously reported impedance spectroscopy observations, where the two semicircles describing the bulk and grain boundary effect can be distinguished clearly in the complex plane,<sup>30</sup> only one strongly suppressed arc is observed in our experimental results. However, the curvature of the left high-frequency arc is larger than that of the right low-frequency arc. This observation can be attributed to the strong overlapping of the bulk and grain boundary semicircles due to the similar time constants between these two relaxation processes.<sup>31</sup> The left high-frequency and right low-frequency components correspond to the bulk and grain boundary effect, respectively.<sup>32,33</sup> The straight line at the right corner of the complex impedance should be a consequence of the contact effect among the sample and Mo film microcircuits.<sup>34</sup>

To quantify the pressure effect on the electrical transport properties of  $\text{Alq}_3$ , the impedance spectra were fitted with a common equivalent circuit model, in which two parallel resistors ( $R$ ) and constant-phase elements (CPE) (Fig. 1b) were introduced to describe the bulk and grain boundary relaxation processes, respectively, on the Zview2 impedance analysis software. The non-ideality of the complex impedance is accounted for by the use of CPE elements, which may affect the reliability of the capacitance or inductance value, while the resistance remains unaffected. The obtained bulk ( $R_b$ ) and grain boundary resistances ( $R_{gb}$ ) are plotted in Fig. 1d. The  $R_b$  of  $\text{Alq}_3$  increases markedly at low pressures ( $<3.1$  GPa), followed by a

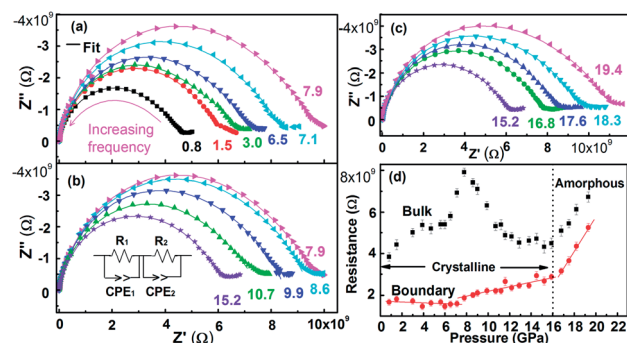


Fig. 1 (a–c) Complex impedance plots of  $Z''$  *vs.*  $Z'$  of  $\text{Alq}_3$  under compression. Lines are the fitted results with the equivalent circuit models describing the bulk ( $R_1$ -CPE<sub>1</sub>) and grain boundary ( $R_2$ -CPE<sub>2</sub>) effects shown in the inset of b. The fitting error is less than 5%. (d) Pressure dependence of the obtained bulk and grain boundary resistances of  $\text{Alq}_3$ .

shoulder from 3.1 to 5.7 GPa, and continues the increasing tendency up to 7.9 GPa. However, with continuous compression, the pressure dependence turns around and  $R_b$  drops rapidly below 15.9 GPa. A similar shoulder in the pressure range of 3.1–6.1 GPa has also been observed in the photoluminescence spectra of  $\text{AlQ}_3$ .<sup>25,26</sup> In contrast,  $R_{gb}$  varies smoothly below 16.4 GPa. Above 16.4 GPa, both  $R_b$  and  $R_{gb}$  increase dramatically with pressure.

We were motivated to find out the mechanism behind the anomalous variation of the electrical transport properties of  $\text{AlQ}_3$  under compression. A discontinuous variation in the electrical transport property of materials usually coincide with the instability of their crystal structure.<sup>35,36</sup> High-pressure XRD measurements were conducted on  $\text{AlQ}_3$  up to 17.4 GPa for the *in situ* observation of the structural modification and selected patterns are shown in Fig. 2. At room conditions, a triclinic crystal structure with  $P\bar{1}$  symmetry ( $\beta\text{-AlQ}_3$ ) appears to be more suitable for the structure of  $\text{AlQ}_3$ . The inset of Fig. 2 shows the structure model of  $\text{AlQ}_3$ . It is surprising that below 16.1 GPa, there is no obvious variation in the patterns of  $\text{AlQ}_3$ , except for the relative peak broadening and the collective movements of all reflection peaks toward a lower  $d$ -spacing. Above 16.1 GPa, all the diffraction peaks lose their intensity, which indicates that  $\text{AlQ}_3$  becomes amorphous. After quenching to ambient pressure, all the reflection peaks re-emerge (Fig. 2), indicating that the amorphization process is reversible. However, it is found that when the sample is pressurized up to 23.8 GPa and then quenched to ambient pressure the pattern disappears, which shows its irreversible character.

To further explore the underlying mechanism and probe the subtle changes of the structures, we conducted high-pressure Raman spectroscopy measurements on  $\text{AlQ}_3$ . As shown in Fig. 3 and 4, in the low pressure range of 0.3–6.9 GPa, no obvious change but the blue-shift, varied relative intensity, and broadening of the vibration Raman modes can be observed. However, above 8.6 GPa, the low-frequency vibration modes in the range of 50–200  $\text{cm}^{-1}$  lose their intensity. The disappearance tendency expands to the higher-frequency vibration modes with further compression. All the Raman vibration modes

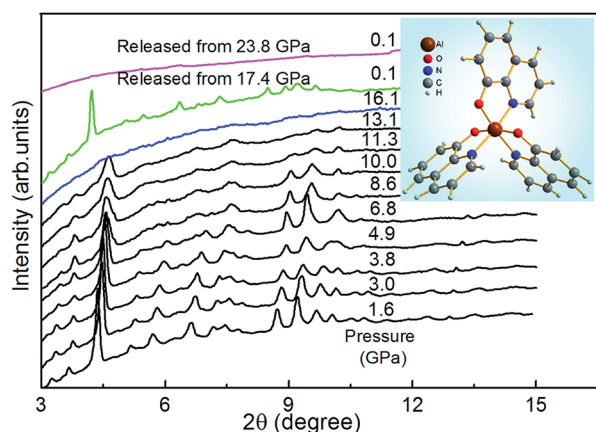


Fig. 2 Representative XRD patterns of  $\text{AlQ}_3$  at various pressures ( $\lambda = 0.6199 \text{ \AA}$ ). The inset shows the structural model of  $\text{AlQ}_3$ .

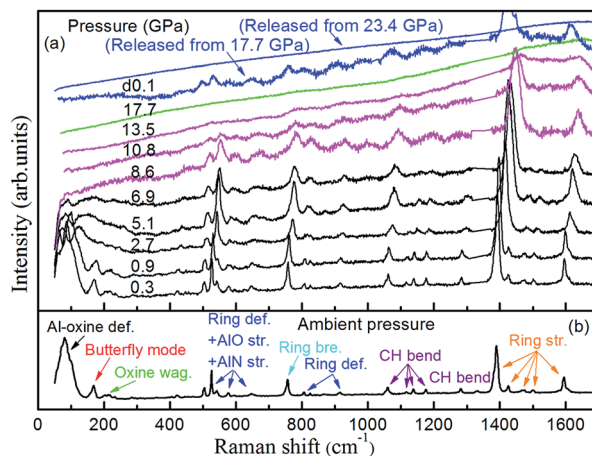


Fig. 3 High-pressure Raman spectra of  $\text{AlQ}_3$  with the Raman peaks of diamond at  $\sim 1331 \text{ cm}^{-1}$  subtracted. Here, def., wag., str., and bre. represent the deformation, wagging, stretching, and breathing vibration modes, respectively.

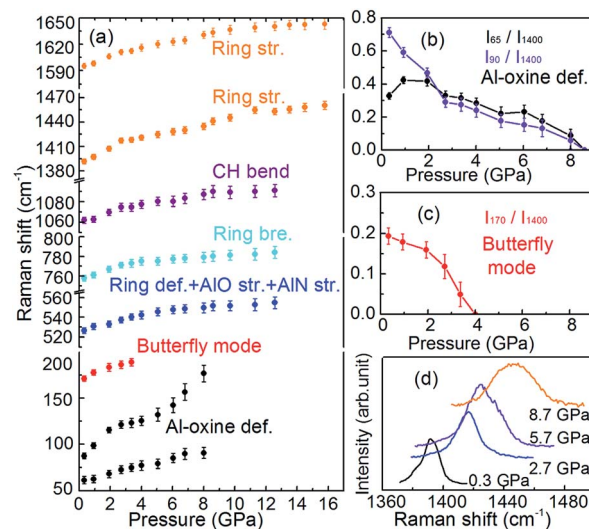


Fig. 4 (a) Pressure dependence of the positions of Raman peaks of  $\text{AlQ}_3$ . (b and c) The ratio of the intensity of the Raman vibration modes at  $\sim 65 \text{ cm}^{-1}$ ,  $\sim 90 \text{ cm}^{-1}$ , and  $\sim 170 \text{ cm}^{-1}$  to the  $\sim 1400 \text{ cm}^{-1}$  mode in  $\text{AlQ}_3$  as a function of pressure. (d) The variation of the Raman peak width ( $\sim 1400 \text{ cm}^{-1}$ ) under pressure.

disappear at  $\sim 17.7 \text{ GPa}$ . The lost Raman vibration modes of  $\text{AlQ}_3$  reappear when the sample is decompressed from 17.7 GPa, but disappear when decompressed to 23.4 GPa, which agrees well with the XRD observation that  $\text{AlQ}_3$  becomes amorphous above 16.1 GPa, and the amorphous process is reversible in the compression below 17.4 GPa but irreversible if compressed to a higher pressure, e.g. 23.8 GPa. This observation can be attributed to the crystalline topology effect.<sup>37,38</sup> At relative low pressures, the crystalline topology of  $\text{AlQ}_3$  (including the atomic coordination and bonding) is preserved, which retains a “memory” of its original crystal structure and can revert to it when releasing pressure to ambient conditions. Upon further compression, the relative higher density amorphous state can

be achieved, which involves some bond breaking, and the broken bonds cannot recover to their original state during decompression. Consequently, the pressure-induced amorphization shows an irreversible character.

Raman studies revealed the subtle structural changes of  $\text{AlQ}_3$  under pressure. At room conditions, the Raman vibration modes of  $\text{AlQ}_3$  have been well assigned<sup>39,40</sup> (Fig. 3b). As clearly shown in Fig. 4, above 8.0 GPa, the Raman active modes lose their intensity gradually from the low- to high-frequency range, which indicates that the Al–oxine bonding is firstly tuned, and then the oxine ligands lose their long-distance ordering, followed by the modification of the ring and C–H bonds with increasing pressure. We infer that the relative Raman intensity changes of the Al–oxine vibration modes (Fig. 4) are caused by the pressure-induced modification of the Al–oxine bonding and the non-planar conformation of the  $\text{AlQ}_3$  molecules. The application of pressure promotes the molecular modification from a non-planar to a planar state, which was observed on other non-planar metal–organic frameworks in previous studies.<sup>41,42</sup>

To further study the effect of compression on the grain boundary, we performed high-resolution transmission electron microscopy (TEM) on  $\text{AlQ}_3$ , which can directly inspect detailed atomic information, and hence is reliable to identify the grain boundaries. Fig. 5 shows the TEM images of the samples that were decompressed from 7, 11 and 17 GPa. It can be found that the average grain size of  $\text{AlQ}_3$  changes smoothly from ambient pressure to 7 GPa, while it decreases significantly at 11 GPa, and becomes smaller at 17 GPa, thus indicating the increase in grain boundary density with applied compression.

The information about the structural evolution under compression is helpful for understanding the complicated electrical transport properties of  $\text{AlQ}_3$ . In the low pressure region (below 8.0 GPa), the crystal structure of  $\text{AlQ}_3$  remains

relatively stable. Therefore, the grain boundary density should be dynamically balanced, and the boundary carrier scattering effect remains almost unchanged. Consequently,  $R_{\text{gb}}$  varies smoothly with pressure. Above 8.0 GPa, the Al–oxine deformation modes of  $\text{AlQ}_3$  lose their intensity, which signal the essential changes in the Al–oxine bonding. The bonding changes connect with the deformation of the  $\text{AlQ}_3$  molecules, and subsequently affect the grain boundary density and the grain boundary disordering, which strengthen the boundary charge carrier scattering effect, and accordingly the  $R_{\text{gb}}$  of  $\text{AlQ}_3$  increases gradually with pressure. Above 16.4 GPa,  $\text{AlQ}_3$  becomes amorphous, which results in the sharp increase of the grain boundary density and structural disordering. As a consequence, the charge carrier scattering effect of the grain boundary is strengthened, which further hinders the boundary conduction of  $\text{AlQ}_3$ .

In the case of bulk electrical transport, it is shown in previously reported studies that  $\pi$ – $\pi$  stacking interactions play important roles in the electrical transport properties of  $\text{AlQ}_3$ .<sup>9,13,14</sup> Under compression, the  $\pi$ – $\pi$  stacking interaction is modified, which is critical to increase the charge transfer rate and charge mobility, and hence facilitate the electrical transport of  $\text{AlQ}_3$ .<sup>13</sup> Therefore, the electrical conductivity of  $\text{AlQ}_3$  should be improved, while it is not consistent with the measured  $R_{\text{b}}$  of  $\text{AlQ}_3$  with compression at 1.6–7.9 GPa. We infer that besides the above mentioned factor, some other factors also affect the electrical transport properties of  $\text{AlQ}_3$ . The similar change tendency between the Al–oxine deformation mode (at  $\sim 90 \text{ cm}^{-1}$ , shown in Fig. 4) and  $R_{\text{b}}$  below 8.0 GPa is a hint of their correlation. Another evidence to support their correlation can be observed from ref. 10, which states that the bonding lengths and angles between the central cation and oxine ligand can heavily affect the electronic structure of  $\text{AlQ}_3$ .<sup>10</sup> This observation can be understood as follows: at ambient pressure, the sample has the low symmetry of a crystal structure in which each of the three Al–oxine ligands (including the Al–O and Al–N bonds) has different bond lengths and angles, and the charges are not uniformly localized on the three ligands.<sup>8</sup> The bonding conformation makes the Al–oxine interaction sensitive to pressure. Under compression, the Al–oxine bonding, especially the Al–N and Al–O bonding lengths and angles are modified considerably, which may enhance the localization of the charge carriers, and thus hinder the conduction of  $\text{AlQ}_3$ . Moreover, pressure-induced defects and structural disordering, which are reflected by the broadening in the Raman spectra and XRD peaks of  $\text{AlQ}_3$  under compression, usually trap the charge carriers and act as recombination centers and can also affect the electrical transport properties of  $\text{AlQ}_3$ . Thus, the  $R_{\text{b}}$  of  $\text{AlQ}_3$  increases with uploading pressure. Above 8.0 GPa, the essential changes in the Al–oxine interaction fundamentally modify the electronic structure of  $\text{AlQ}_3$  and drive the redistribution of electron density between adjacent oxine ligands and the localized-delocalized charge transfer, which combine with the improved conduction due to the enhanced  $\pi$ – $\pi$  stacking interaction and non-planar to more-planar conformation modification under compression, offsets the hindering effect of structural disorder or defects and makes  $\text{AlQ}_3$  more conductive.

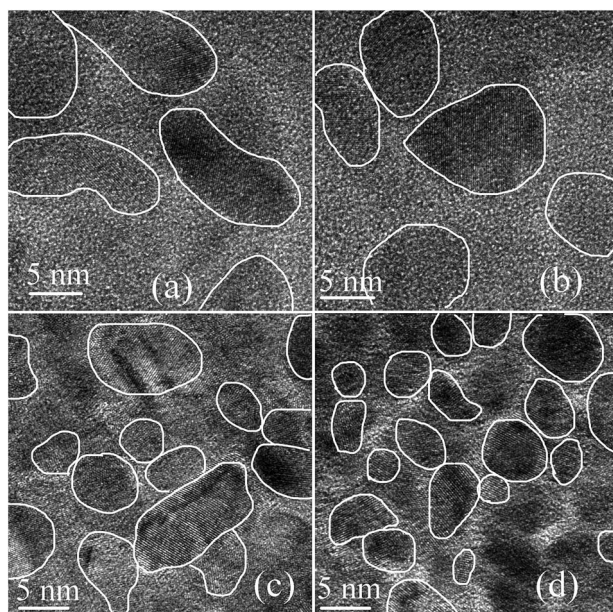


Fig. 5 High-resolution transmission electron microscopy images of  $\text{AlQ}_3$  quenched at different pressures: (a) ambient pressure, (b) 7 GPa, (c) 11 GPa and (d) 17 GPa.

The dramatic increase of  $R_b$  above 16.4 GPa is induced by the amorphization process, which brings about a higher degree of structural disorder and significantly reduces the free travelling distances of the charge carriers. The experimental results suggest that the Al–oxine interaction also plays an important role on the electrical transport properties of Alq<sub>3</sub>.

## Conclusions

By combing XRD, Raman spectroscopy, TEM and impedance spectra measurements, we have studied the electrical transport and structural properties of compressed Alq<sub>3</sub>, an extensively used electron transport material in OLEDs. The  $R_b$  of Alq<sub>3</sub> increases with uploading pressure, while it decreases markedly at pressures above 8.6 GPa. In contrast, the  $R_{gb}$  changes smoothly below 16.4 GPa. With further compression, both the  $R_b$  and  $R_{gb}$  increase dramatically along with the amorphization of Alq<sub>3</sub>. The pressure-induced amorphization is reversible at a low density amorphous state but irreversible at a relatively higher density state. Interestingly, XRD measurements indicate that there is no structural transition at ~8.0 GPa, which is the pressure at which  $R_b$  reaches the maximum. The tendency reversal is found to be synchronous with the Raman shift of the Al–oxine deformation vibration modes, which rationalizes the anomalous changes of the electrical transport behavior. Besides the contribution of  $\pi$ – $\pi$  stacking interactions, the Al–oxine interaction is believed to be also important for the transport properties on dense Alq<sub>3</sub>, which provides essential insight into the correlation between structural modification and electrical properties, and establishes general guidelines for designing or optimizing new Alq<sub>3</sub>-based applications.

## Acknowledgements

The authors thank M. Zhou (College of physics, Jilin University, China) for discussion. This work was supported by the National Basic Research Program of China (Grant no. 2011CB808204), the National Natural Science Foundation of China (Grant nos 11374121 and 11404133), the China Postdoctoral Science Foundation (Grant no. 2013M540243), and the Program of Science and Technology Development Plan of Jilin Province (Grant no. 20140520105JH).

## Notes and references

- 1 C. W. Tang and S. A. VanSlyke, *Appl. Phys. Lett.*, 1987, **51**, 913.
- 2 J. M. Shi and C. W. Tang, *Appl. Phys. Lett.*, 1997, **70**, 1665.
- 3 H. Aziz and Z. D. Popovic, *Chem. Mater.*, 2004, **16**, 4522.
- 4 S. Berleb and W. Brutting, *Phys. Rev. Lett.*, 2002, **89**, 286601.
- 5 H. Aziz, Z. D. Popovic, N. X. Hu, A. M. Hor and G. Xu, *Science*, 1999, **283**, 1900.
- 6 M. S. Xu and J. B. Xu, *Thin Solid Films*, 2005, **491**, 317.
- 7 M. Muccini, M. A. Loi, K. Kenevey, R. Zamboni, N. Masciocchi and A. Sironi, *Adv. Mater.*, 2004, **16**, 861.
- 8 A. Curioni, M. Boero and W. Andreoni, *Chem. Phys. Lett.*, 1998, **294**, 263.
- 9 B. C. Lin, C. P. Cheng, Z. Q. You and C. P. Hsu, *J. Am. Chem. Soc.*, 2005, **127**, 66.
- 10 F. F. Muhammad, A. I. A. Hapip and K. J. Sulaiman, *J. Organomet. Chem.*, 2010, **695**, 2526.
- 11 M. Rajeswaran and T. N. Blanton, *J. Chem. Crystallogr.*, 2005, **35**, 71.
- 12 J. S. Jiang, J. E. Pearson and S. D. Bader, *Phys. Rev. B: Condens. Matter Mater. Phys.*, 2008, **77**, 035303.
- 13 B. C. Lin, C. P. Cheng, Z. Q. You and C. P. Hsu, *Phys. Chem. Chem. Phys.*, 2011, **13**, 20704.
- 14 A. Fuchs, T. Steinbrecher, M. S. Mommer, Y. Nagata, M. Elstner and C. Lennartz, *Phys. Chem. Chem. Phys.*, 2012, **14**, 4259.
- 15 M. Brinkmann, G. Gadret, M. Muccini, C. Taliani, N. Masciocchi and A. Sironi, *J. Organomet. Chem.*, 2000, **122**, 5147.
- 16 M. Colle, R. E. Dinnebier and W. Brutting, *Chem. Commun.*, 2002, 2908.
- 17 H. Bi, D. Chen, D. Li, Y. Yuan, D. D. Xia, Z. L. Zhang, H. Y. Zhang and Y. Wang, *Chem. Commun.*, 2011, **47**, 4135.
- 18 M. Goswami, P. K. Nayak, N. Periasamy and P. K. Madhu, *Chem. Cent. J.*, 2009, **3**, 15.
- 19 M. Rajeswaran, T. N. Blanton, R. H. Young and W. Brennessel, *J. Chem. Crystallogr.*, 2010, **40**, 195.
- 20 M. Rajeswaran, T. N. Blanton, C. W. Tang, W. C. Lenhart, S. C. Switalski, D. J. Giesen, B. J. Antalek, T. D. Pawlik, D. Y. Kondakov, N. Zumbulyadis and R. H. Young, *Polyhedron*, 2009, **28**, 835.
- 21 M. Colle, J. Gmeiner, W. Milius, H. Hillebrecht and W. Brutting, *Adv. Funct. Mater.*, 2003, **13**, 108.
- 22 H. Bi, H. Y. Zhang, Y. Zhang, H. Z. Gao, Z. M. Su and Y. Wang, *Adv. Mater.*, 2010, **22**, 1631.
- 23 P. Dera, C. T. Prewitt, S. Japel, D. L. Bish and C. T. Johnston, *Am. Mineral.*, 2003, **88**, 1428.
- 24 P. Destruel, P. Jolinat, R. Clergereaux and J. Farenc, *J. Appl. Phys.*, 1999, **85**, 397.
- 25 I. Hernandez and W. P. Gillin, *J. Phys. Chem. B*, 2009, **113**, 14079.
- 26 I. Hernandez, W. P. Gillin and M. Somerton, *J. Lumin.*, 2009, **129**, 1835.
- 27 Q. L. Wang, Y. H. Han, C. L. Liu, Y. Z. Ma, W. B. Ren and C. X. Gao, *Appl. Phys. Lett.*, 2012, **100**, 172905.
- 28 Y. Wang, Y. H. Han, C. X. Gao, Y. Z. Ma, C. L. Liu, G. Peng, B. J. Wu, B. Liu, T. J. Hu, X. Y. Cui, W. B. Ren, Y. Li, N. N. Su, H. W. Liu and G. T. Zou, *Rev. Sci. Instrum.*, 2010, **81**, 013904.
- 29 H. K. Mao, P. M. Bell, J. W. Shaner and D. J. Steinberg, *J. Appl. Phys.*, 1978, **49**, 3276–3283.
- 30 C. Y. He, C. X. Gao, Y. Z. Ma, M. Li, A. M. Hao, X. W. Huang, B. G. Liu, D. M. Zhang, C. L. Yu, G. T. Zou, Y. C. Li, H. Li, X. D. Li and J. Liu, *Appl. Phys. Lett.*, 2007, **91**, 092124.
- 31 R. Schmidt, J. Wu, C. Leighton and I. Terry, *Phys. Rev. B: Condens. Matter Mater. Phys.*, 2009, **79**, 125105.
- 32 J. C. C. Abrantes, J. A. Labrincha and J. R. Frade, *Mater. Res. Bull.*, 2000, **35**, 727.
- 33 I. Denk, J. Claus and J. Maier, *J. Electrochem. Soc.*, 1997, **144**, 3526.

- 34 H. L. Tuller, *Solid State Ionics*, 2000, **131**, 143.
- 35 A. P. Nayak, S. Bhattacharyya, J. Zhu, J. Liu, X. Wu, T. Pandey, C. Q. Jin, A. K. Singh, D. Akinwande and J.-F. Lin, *Nat. Commun.*, 2014, **5**, 3731.
- 36 T. Matsuoka and K. Shimizu, *Nature*, 2009, **458**, 186.
- 37 Y. H. Hu and L. Zhang, *Phys. Rev. B: Condens. Matter Mater. Phys.*, 2010, **81**, 174103.
- 38 I. Peral and J. Iniguez, *Phys. Rev. Lett.*, 2006, **97**, 225502.
- 39 M. D. Halls and R. Aroca, *Can. J. Chem.*, 1998, **76**, 1730.
- 40 M. Braun, J. Gmeiner, M. Tzolov, M. Coelle, F. D. Meyer, W. Milius, H. Hillebrecht, O. Wendland, J. U. Von Schutz and W. Brutting, *J. Chem. Phys.*, 2001, **114**, 9625.
- 41 M. Zhou, K. Wang, Z. W. Men, C. L. Sun, Z. L. Li, B. B. Liu, G. T. Zou and B. Zou, *CrystEngComm*, 2014, **16**, 4084.
- 42 M. Zhou, M. J. Sun, Z. W. Men, Z. L. Li, T. C. Liu, Y. Z. Chen, S. N. Sun, C. L. Sun, S. Q. Gao and Z. W. Li, *J. Phys. Chem. B*, 2013, **117**, 8911.